Electrostatic interactions with dielectric samples in scanning probe microscopies

Ali Sadeghi,* Alexis Baratoff, and Stefan Goedecker
Departement Physik, Universität Basel, Klingelbergstrasse 82, CH-4056 Basel, Switzerland
(Received 6 May 2013; published 22 July 2013)

Electrostatic interactions between the conducting tip of a scanning probe microscope and a flat conductor coated with a thin or thick dielectric layer are treated analytically and numerically. Exact and compact approximate expressions for the capacitance, force, force gradient, electric field profiles, and their effective widths are derived for a spherical model tip by generalizing known solutions for the conducting sphere and sample problem. These expressions allow convenient modeling of various measurements involving voltage-biased probes, estimation of lateral resolution, and prediction of trends as a function of relevant parameters.

DOI: 10.1103/PhysRevB.88.035436 PACS number(s): 73.40.Ns, 07.79.−v, 41.20.Cv, 68.37.−d

I. INTRODUCTION

Three decades after the invention of the scanning tunneling microscope (STM),[1] diverse scanning probe microscopy (SPM) techniques have become available for the study of local chemical and physical surface properties of materials as well as for manipulating them down to the atomic scale. Unlike STM, scanning force microscopy[2] (SFM) can be applied to dielectric samples.[3] Among various interactions with the probing tip, the ubiquitous long-range electrostatic (ES) force is of special importance in SPM techniques involving voltage-biased conducting tips.[4] In electrostatic force microscopy (EFM)[5] the ES force is directly measured, whereas in Kelvin probe force microscopy (KPFM)[6] the contact potential difference (CPD) is mapped by compensating an ac signal related to the ES force. Those techniques, as well as scanning capacitance microscopy (SCM), can be used to determine the local charging properties of dielectric samples or surface layers and of semiconductor devices protected by insulating layers. In particular, two-dimensional electron gas (2DEG)-based structures can be controlled by voltages applied to a back electrode (gate) and to top gates confining the 2DEG laterally. SCM is being extensively used to map lateral doping profiles,[7] but can also detect the *quantum capacitance* due to the occupation of confined electronic states, e.g., in the quantum Hall effect.[8] Furthermore, scanning gate microscopy (SGM) studies, where a biased conducting tip locally perturbs electron waves or shifts the levels of confined states past the Fermi energy, have allowed one to map induced variations in the conductance of quantum constrictions,[9] quantum dots,[10] and of increasingly complex structures of current interest.

Typical insulator thickness h, tip radius R, and average tip-sample distance s being of the same order (tens of nanometers) in such measurements, their lateral resolution has often been roughly assumed to be $\sim R$. Although three-dimensional (3D) numerical solutions of the Poisson equation yield an accurate description of the tip-induced electrostatic potential for each particular probe-sample geometry, analytic expressions for the capacitance, the ES force, and its vertical gradient as functions of R, s, and h are highly desirable. The same holds also for the electric field profiles at the top and bottom surfaces of a uniform dielectric layer in contact with a flat back electrode. Their widths provide useful estimates of the lateral resolution of local CPD or surface charge variations, but also of tip-induced conductance changes in buried semiconductor devices, at least if the field distribution at the interface is narrower than the structure lateral dimensions but exceeds the lateral screening length.

For flat conducting samples, Hudlet *et al.*[11] proposed an approximate analytic model which is surprisingly accurate, also for atomically thin insulating layers on metals.[12] Dielectric samples or layers on a conducting back electrode, however, have been predominately simulated numerically because of the complexity introduced by partial field penetration (see, e.g., Refs. 13 and 14 and references therein). In this paper we obtain exact and novel approximate analytic results for a spherical model tip facing such a slab. The derived expressions can be used for further analysis of experiments on the above-mentioned types of samples. Our formalism can also be generalized to multilayer slabs.

II. SPHERICAL TIP ATOP A SEMI-INFINITE DIELECTRIC

The classical electric potential between a cylindrically symmetric conducting probe at potential V facing a dielectric slab grounded on the bottom can be calculated by means of the image charges method. In order to obtain an analytic solution, we model the tip as a sphere of the same radius R as the apex, see Fig. 1(a). Additional contributions to the capacitance C and the ES force F from the tip shank and the supporting sensor can be important for thick dielectric slabs.[14] However, they vary more slowly than the contribution from the tip apex, so that our approximation captures the main features of ES properties at tip-sample distances $s < R$.

The problem of a sphere facing a semi-infinite dielectric is solved by combining two textbook problems,[15] namely a point charge q at a distance r from the center of the conducting sphere or at a distance z_q from the surface of the dielectric. If an image charge $-qR/r$ is placed at a distance R^2/r from the sphere center on the same radial line as q, the sphere surface is an equipotential. In the second problem, the electric potential outside the dielectric can be obtained by adding the Coulomb potentials of q and of an image charge $-\beta q$ at $-z_q$ on the normal to the surface, where

$$\beta = \frac{\epsilon - \epsilon_0}{\epsilon + \epsilon_0},$$

ϵ and ϵ_0 being the permittivities of the dielectric and of vacuum (or that of the external medium), respectively. The potential inside the dielectric is that of single point charge $(1 - \beta)q$

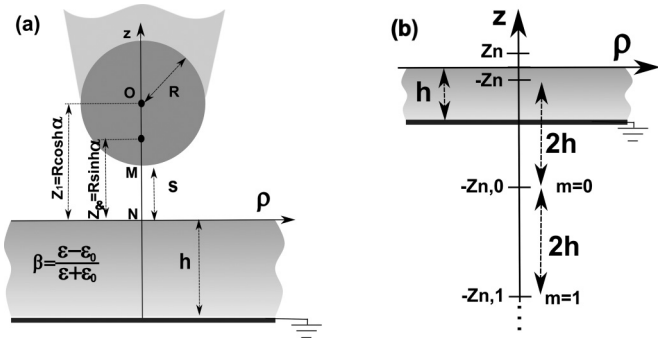

FIG. 1. (a) The probe tip modeled as a conducting sphere of the same radius R as its apex at a separation s from a dielectric slab of thickness h. The tip is biased at V while the bottom back electrode is grounded. Image charges which sum up to the charge on the sphere are located between z_1 and z_∞. (b) Positions of image charges below the surface of the dielectric slab due to a point charge at z_n.

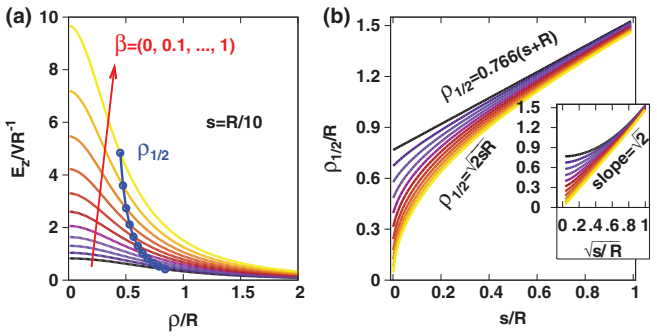

FIG. 2. (Color online) (a) Lateral profile of the perpendicular field component just outside the sample and its half-width $\rho_{1/2}$ (blue dots) for a conducting sphere of radius R separated by $s = 0.1R$ from a semi-infinite dielectric. (b) Variation of $\rho_{1/2}/R$ against s/R and $\sqrt{s/R}$ (inset); the curves are bounded by $\rho_{1/2} = \sqrt{2Rs}$ at small s/R for $\beta = 1$ and $\rho_{1/2} = 0.766(s + R)$ for $\beta = 0$ or at large s/R for all β.

at z_q if that region were vacuum [or equivalently, of a point charge $(1 + \beta)q$ at z_q if the whole space were filled with the dielectric]. Physically, each image charge represents the effect of the polarization induced at the surface of the sphere or of the dielectric.

In the combined problem, i.e., sphere against dielectric, a charge $q_1 = 4\pi\epsilon_0 RV$ located at the center of the sphere ($z_1 = R + s$) tends to make the surface of the sphere an equipotential at V. The image $-\beta q_1$ at $-z_1$ below the dielectric surface, however, modifies the potential on the sphere surface. A second charge $q_2 = \beta q_1 R/2z_1$ is then placed at $z_2 = z_1 - R^2/2z_1$ to bring the sphere potential towards V, which induces in turn an image $-\beta q_2$ at $-z_2$ and so forth. The resulting convergent series of point charges inside the sphere

$$q_{n+1} = \frac{\beta q_n R}{z_1 + z_n} \quad (q_1 = 4\pi\epsilon_0 RV), \tag{1}$$

$$z_{n+1} = z_1 - \frac{R^2}{z_1 + z_n} \quad (z_1 = R + s), \tag{2}$$

together with their corresponding images below the dielectric surface $\{-\beta q_n, -z_n\}$ satisfy the boundary conditions both on the sphere and dielectric surfaces. The attractive force on the sphere can be obtained by summing the Coulomb forces between the charges inside the sphere and their images inside the dielectric

$$F(s,V) = \frac{1}{4\pi\epsilon_0} \sum_{n,n'=1}^{\infty} \frac{-\beta q_n q_{n'}}{|z_n + z_{n'}|^2}. \tag{3}$$

The Green's function (GF) is

$$G_n^{\pm} = \frac{1}{\sqrt{\rho^2 + (z - z_n)^2}} - \frac{\beta}{\sqrt{\rho^2 + (z \pm z_n)^2}}, \tag{4}$$

where G_n^+ and G_n^- refer to $z \geqslant 0$ and $z \leqslant 0$ regions, respectively. The electric potential $\Phi(\rho,z) = \frac{1}{4\pi\epsilon_0} \sum q_n G_n$ and the electric field $\mathbf{E} = \frac{-1}{4\pi\epsilon_0} \sum q_n \nabla G_n$ can be obtained outside the sphere, above or inside the dielectric slab.

A. Electric field profile

The z component of the electric field just above the surface of the sample ($z = 0$)

$$E_z = \frac{1 + \beta}{4\pi\epsilon_0} \sum_{n=1}^{\infty} \frac{q_n z_n}{(\rho^2 + z_n^2)^{3/2}} \tag{5}$$

is especially relevant in AFM and STM experiments because it polarizes atoms or ions and thus set up microscopic local fields which influence atomic-scale contrast.[16] For tip-sample separations s where such contrast appears, E_z approaches a uniform value $E_N \equiv E_z(\rho = 0)$ and can be inserted into atomistic model potential[16,17] or *ab initio* simulations.[14]

Figure 2(a) shows how E_z gradually weakens as ρ increases. Its effective width can be characterized by $\rho_{1/2}$ at which $E_z = E_N/2$. When $\beta \simeq 0$ as well as for $s \gtrsim R$, $\rho_{1/2}$ approaches the point-charge-like asymptotic linear relation $\sqrt{2^{2/3} - 1}(R + s) \simeq 0.766(R + s)$, as can be seen in Fig. 2(b). Over a perfect conductor ($\beta = 1$), on the other hand, $\rho_{1/2} \simeq \sqrt{2Rs}$ for sufficiently small s/R, as seen in the inset, hence formally vanishes upon contact because E_N then becomes infinite. Keeping in mind that for commonly used solid dielectrics[18] $\beta \geqslant 0.6$, the behavior highlighted in the inset indicates that $\rho_{1/2}$ *is considerably smaller than* R *if* $s \ll R$.

An alternative definition of the half-width directly related to the capacitance is based on the charge distribution at each surface. We define an effective area S^* such that

$$q^* = \int_S D_\perp dS \equiv D_\perp^* S^*,$$

where q^* is the total charge on the surface of area S, $D_\perp$ is the normal component of the electric displacement vector, and $D_\perp^* \equiv D_{\perp,\max}$. First we calculate the angular half-width θ_C for a conducting sphere separated by s from a semi-infinite dielectric. We have

$$q^* = \sum_{n=1}^{\infty} q_n, \quad S^* = 2\pi R^2(1 - \cos\theta_C),$$

$$D_\perp^* = \epsilon_0 E_z(0,s) = \frac{1}{4\pi} \sum_{n=1}^{\infty} q_n \left[\frac{1}{(z_n - s)^2} + \frac{\beta}{(z_n + s)^2} \right].$$

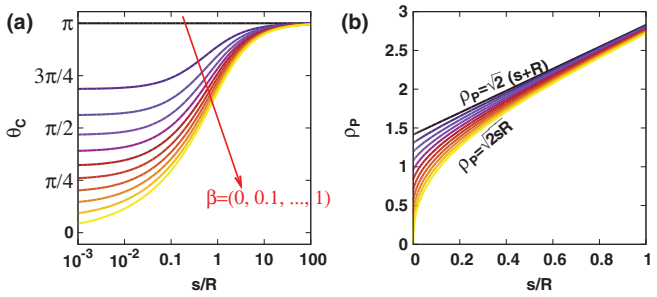

FIG. 3. (Color online) (a) θ_C and (b) ρ_P as a function of s/R for a sphere facing a semi-infinite dielectric. In (b) the curves are bounded by $\rho_P = \sqrt{2}(s+R)$ for $\beta = 0$ and $\rho_P \simeq \sqrt{2sR}$ for $\beta = 1$ and $s \ll R$.

If $\beta = 0$, $z_n - s = R$ and $\theta_C = \pi$ as required for an isolated sphere. For a perfect conductor ($\beta = 1$), on the other hand, $\theta_C \simeq 45^\circ$ at a separation $s = R/10$, as seen in Fig. 3(a). These plots can be used to judge whether the approximation of the tip by a sphere is justified, e.g., θ_C should at least be smaller than 90° minus the cone half-angle for a conical tip terminated by a spherical cap.

Over the sample surface we consider instead the polarization surface charge density $P_\perp = (\epsilon - \epsilon_0)E_z^-(\rho,0)$,[15] where $E_z^-(\rho,0) = \frac{\beta-1}{4\pi\epsilon_0}\sum q_n z_n/(\rho^2+z^2)^{3/2}$, thus

$$q^* = -\beta\sum_{n=1}^{\infty} q_n, \quad S^* = \pi\rho_P^2, \quad P_\perp^* = \frac{-\beta}{2\pi}\sum_{n=1}^{\infty}\frac{q_n}{z_n^2}.$$

Therefore

$$\rho_P = \sqrt{2\sum_{n=1}^{\infty} q_n \Big/ \sum_{n=1}^{\infty}\frac{q_n}{z_n^2}}. \tag{6}$$

For a single point charge at z_n, we obtain $\rho_P = \sqrt{2}z_n$ (independent of β) which also coincides with the value at which the parallel component E_ρ is maximum. When $s \gg R$ or $\beta \ll 1$, ρ_P of the sphere approaches the point-charge-like asymptotic linear behavior, i.e., $\rho_P = \sqrt{2}(s+R)$, because then all charges vanish except q_1 at $z_1 = s + R$. As shown in Fig. 3(b), for a perfect conductor ($\beta = 1$) $\rho_P \simeq \sqrt{2sR}$, i.e., like $\rho_{1/2}$, and is significantly smaller than R if $s \ll R$.

B. Closed-form expressions for capacitance, force, force gradient, and field

Following Ref. 19, one can write Eq. (1) as a second order homogeneous difference equation with constant coefficients

$$\frac{1}{q_n} = \frac{2\cosh\alpha}{\beta}\frac{1}{q_{n-1}} - \frac{1}{\beta^2}\frac{1}{q_{n-2}} \quad (n \geqslant 3)$$

the solution of which is a linear combination of $\exp(\pm n\alpha)$ where

$$\cosh\alpha = \frac{z_1}{R} = 1 + \frac{s}{R}.$$

Substituting the known expressions for q_1 and q_2, we obtain

$$q_n = 4\pi\epsilon_0 RV\sinh\alpha\left(\frac{\beta^{n-1}}{\sinh n\alpha}\right), \tag{7}$$

$$z_n = R\sinh\alpha\coth n\alpha \quad (n \geqslant 1), \tag{8}$$

which are a simple generalization of the solution for a semi-infinite conductor ($\beta = 1$)[19] for arbitrary β and provide a convenient expression for the capacitance

$$C = \frac{1}{V}\sum_{n=1}^{\infty} q_n = 4\pi\epsilon_0 R\sinh\alpha\sum_{n=1}^{\infty}\frac{\beta^{n-1}}{\sinh n\alpha}. \tag{9}$$

Being the capacitance $C_{\rm sph} = 4\pi\epsilon_0 R$ of the sphere alone in vacuum, the constant leading term in C can be ignored because only variations of C (i.e., of $C - C_{\rm sph}$) with tip position are of interest.

Corresponding expression for the attractive electric force on the tip ($F = C'V^2/2$ where $C' = dC/ds$) is given by

$$F = 2\pi\epsilon_0 V^2\sum_{n=2}^{\infty}\frac{\beta^{n-1}}{\sinh n\alpha}(\coth\alpha - n\coth n\alpha). \tag{10}$$

Similarly, the vertical force gradient (dF/ds) is given by

$$F' = \frac{2\pi\epsilon_0 V^2}{R\sinh\alpha}\sum_{n=2}^{\infty}\frac{\beta^{n-1}}{\sinh n\alpha}\left[\frac{n^2}{\sinh^2 n\alpha} - \frac{1}{\sinh^2\alpha} + n\coth n\alpha(n\coth n\alpha - \coth\alpha)\right]. \tag{11}$$

In dynamic EFM or SCM experiments with stiff deflection sensors F' is proportional to the resonance frequency shift which is used to control the tip-sample separation s.[3]

Finally, the maximum electric field outside the surface, i.e., $E_N \equiv E_z(\rho = 0, z = 0)$, reads

$$E_N = \frac{V}{R}\left(\frac{1+\beta}{\sinh\alpha}\right)\sum_{n=1}^{\infty}\frac{\beta^{n-1}\sinh n\alpha}{\cosh^2 n\alpha}. \tag{12}$$

1. Limiting values

Except for $\alpha = 0$ and $\beta = 1$, q_n decays exponentially towards zero. For an ideal conductor ($\beta = 1$) these expressions diverge in the limit $s \to 0$ (i.e., $\alpha \to 0$). For dielectrics, the resulting series for all quantities converge. We obtain $q_n(s=0) = q_1\beta^{n-1}/n$, $z_n(s=0) = R/n$ and

$$C_{\max} = -4\pi\epsilon_0 R\left[\frac{\ln(1-\beta)}{\beta}\right]. \tag{13}$$

Like C, $-F$ and F' are monotonically decreasing functions of s. Their upper bounds attained at $s = 0$ ($\alpha = 0$), namely

$$F_{\max} = -\frac{2}{3}\pi\epsilon_0 V^2\left[\frac{\ln(1-\beta)}{\beta} + \frac{1}{(1-\beta)^2}\right],$$

$$F'_{\max} = \frac{4\pi\epsilon_0 V^2}{45R}\left[\frac{\ln(1-\beta)}{\beta} + \frac{1}{(1-\beta)^2} + \frac{21\beta}{(1-\beta)^4}\right],$$

are finite if $\beta < 1$ as shown in Fig. 4 . The result for $F(s=0)$ is stated without proof in Ref. 20. Finally,

$$E_{N,\max} = \frac{V}{R}\frac{1+\beta}{(1-\beta)^2}.$$

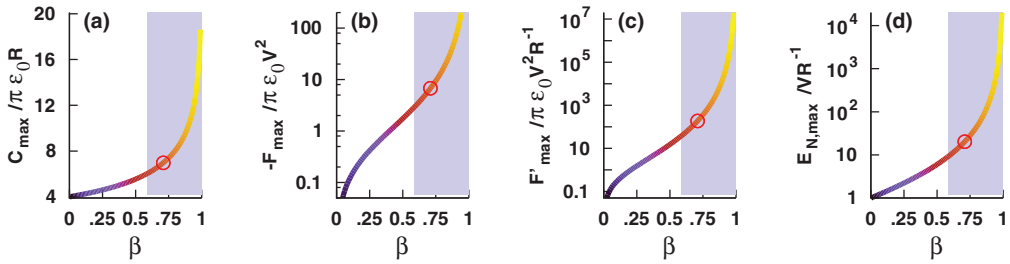

FIG. 4. (Color online) The upper bounds of C, $-F$, F', and E_N (in units $\pi\epsilon_0 R$, $\pi\epsilon_0 V^2$, $\pi\epsilon_0 V^2 R^{-1}$, and VR^{-1}, respectively) as a function of β, attained for a conducting sphere touching ($s = 0$) the semi-infinite dielectric surface. The relevant range for typical values[18] $\beta_{\mathrm{PMMA}} \simeq \beta_{\mathrm{SiO_2}} = 0.59$, $\beta_{\mathrm{NaCl}} = 0.71$ (circles), $\beta_{\mathrm{Al_2O_3}} = 0.80$, $\beta_{\mathrm{Si}} = 0.86$, $\beta_{\mathrm{HfO_2}} = 0.92$, and $\beta_{\mathrm{LiNbO_3}} = 0.93$–$0.98$, is shaded.

They all provide useful upper bounds on the corresponding quantities in case of a realistic probe tip of apex radius R.[14] Their dependences on β are plotted in Fig. 4. As an example, the limiting values for NaCl ($\epsilon_r = 5.9$, $\beta = 0.71$) are $C_{\max}/\pi\epsilon_0 R = 6.98$, $F_{\max}/\pi\epsilon_0 V^2 = -6.77$ (i.e., $F_{\max} = -0.188\ \mathrm{nN/V^2}$ independent of the sphere radius), $F'_{\max}/\pi\epsilon_0 V^2 R^{-1} = 188.7$ and $E_{N,\max}/VR^{-1} = 20.4$.

2. Approximate expressions

For $s/R < 0.1$ many terms in Eqs. (9)–(12) are required to get a reasonable accuracy. However, the truncation error is dramatically reduced, as illustrated in Table I, by adapting a procedure proposed for the sphere-conductor problem.[21] Equation (8) shows that z_n approaches $z_\infty = R\sinh\alpha$ as $\exp(-2n\alpha)$, whereas q_n decays as $\beta^{n-1}\exp(-n\alpha)$. If the charge series is truncated at some q_k for which $z_{n>k} \simeq z_\infty$, the remainder can be summed up analytically as a correction term

$$q^{(k)}_{\mathrm{corr}} \equiv \sum_{n=k+1}^{\infty} q_n \simeq \frac{q_{k+1}}{1-\beta e^{-\alpha}} = \frac{q_1\beta^k/(1-\beta e^{-\alpha})}{\sinh[(k+1)\alpha]/\sinh\alpha} \tag{14}$$

lumped at z_∞ where we have used $q_{n+1}/q_{n>k} \simeq \beta R/(z_1 + z_\infty) = \beta e^{-\alpha}$. Moreover, Eq. (14) leads to compact, accurate analytical expressions. For example,

$$C^{(1)} - C_{\mathrm{sph}} \simeq 2\pi\epsilon_0 R\left[\frac{\beta/(1-\beta e^{-\alpha})}{\cosh\alpha}\right], \tag{15}$$

$$C^{(2)} - C_{\mathrm{sph}} \simeq 2\pi\epsilon_0 R\left[\frac{\beta}{\cosh\alpha} + \frac{\beta^2/(1-\beta e^{-\alpha})}{4\cosh^2\alpha - 1}\right] \tag{16}$$

approximate Eq. (9) within 5% and 1%, respectively, as seen in Table I.

Our formulas should be useful in theoretical modeling and data interpretation. Without the correction, Eq. (16) becomes $2\pi\epsilon_0 R\beta/(1 + s/R)$ with an error larger than 33% at $s = R/10$. However, it gives the correct asymptotic behavior $C - C_{\mathrm{sph}} = 2\pi\epsilon_0\beta R^2/s$ for $s \gg R$. The prefactor of the approximation proposed by Hudlet *et al.*[11] for a conducting sample, i.e.,

$$C - C_{\mathrm{sph}} = 2\pi\epsilon_0 R\ln\left(1 + \frac{R}{s}\right), \tag{17}$$

was adjusted to match this asymptotic behavior, although their basic assumption (constant field along field lines perpendicular to the sphere and sample surfaces) is reasonable only for small s/R. Nevertheless, Eq. (17) is remarkably accurate at moderate separations, as demonstrated in the last column of Table I.

III. POINT CHARGE ABOVE A DIELECTRIC SLAB

Next we consider the intermediate problem of a point charge at ($\rho = 0, z_n \geqslant 0$) against a dielectric slab of thickness h; see Fig. 1(b). When $h \to \infty$, the GF is given by Eq. (4). For finite h, G_n is, however, modified because the field lines become perpendicular to the surface of the back electrode. Appropriate expressions are derived and plots of the resulting field profiles and of their half-widths are presented below. Compared to the treatment in Ref. 22, the GF approach is more convenient, especially for extending to the case of a multilayer slab for which similar boundary conditions are applied at each interface.

A. Green's function

In cylindrical coordinates, the Green's function (GF) above and below the slab surface has the form[15]

$$G^+_n = \int_0^\infty (e^{-k|z-z_n|} + A_1 e^{-kz})J_0(k\rho)dk, \tag{18}$$

$$G^-_n = \int_0^\infty (A_2 e^{-kz} + A_3 e^{+kz})J_0(k\rho)dk, \tag{19}$$

TABLE I. Relative error in calculating C using k point charges in addition to $q^{(k)}_{\mathrm{corr}}$.

	$\beta = 0.71$ (NaCl)				$\beta = 1$ (conductor)				
s/R	$k = 1$	2	10	20	1	2	10	20	Eq. (17)
0.1	0.02	0.004	10^{-7}	10^{-15}	0.05	0.01	10^{-7}	10^{-13}	0.02
0.2	0.008	0.001	10^{-11}	$<10^{-16}$	0.02	0.002	10^{-8}	$<10^{-16}$	0.02
0.5	0.001	10^{-5}	10^{-16}	$<10^{-16}$	0.003	10^{-4}	10^{-14}	$<10^{-16}$	0.01

J_0 being the zero order Bessel function of the first kind. Recall that

$$\int_0^\infty e^{-k|z-z_n|} J_0(k\rho) dk = \frac{1}{\sqrt{\rho^2+(z-z_n)^2}}.$$

The boundary conditions[23]

$$G_n^-(\rho,-h)=0, \quad G_n^+(\rho,0)=G_n^-(\rho,0),$$
$$\left.\frac{\partial G_n^+}{\partial z}\right|_{z=0} = \epsilon_r \left.\frac{\partial G_n^-}{\partial z}\right|_{z=0},$$

determine the coefficients

$$A_1 = -\left(\frac{\beta+e^{-2kh}}{1+\beta e^{-2kh}}\right)e^{-kz_n}, \quad A_2 = -e^{-2kh}A_3,$$
$$A_3 = \left(\frac{1-\beta}{1+\beta e^{-2kh}}\right)e^{-kz_n}.$$

Using

$$\frac{1}{1+\beta e^{-2kh}} = \sum_{m=0}^{\infty}(-\beta)^m e^{-2mkh}$$

we obtain expressions for GF for any field point (ρ,z) above the surface

$$G_n^+ = \frac{1}{\sqrt{\rho^2+(z-z_n)^2}} - \frac{\beta}{\sqrt{\rho^2+(z+z_n)^2}} - (1-\beta^2)\sum_{m=0}^{\infty}\frac{(-\beta)^m}{\sqrt{\rho^2+(z+z_{nm})^2}} \tag{20}$$

and inside the slab

$$G_n^- = (1-\beta)\sum_{m=0}^{\infty}(-\beta)^m\left[\frac{-1}{\sqrt{\rho^2+(z+z_{nm})^2}} + \frac{1}{\sqrt{\rho^2+(z+2h-z_{nm})^2}}\right], \tag{21}$$

where

$$z_{nm} = z_n + 2(m+1)h. \tag{22}$$

Equations (20) and (21) reduce to Eq. (4) for $h\to\infty$, and the GF of a perfect conductor is obtained for $\beta=1$. Above a dielectric slab of finite h, however, G_n^+ includes additional terms because q_n induces, in addition to the first image $-\beta q_n$ at $-z_n$, an infinite sequence of alternating image charges $-(1-\beta^2)(-\beta)^m q_n$ at equidistant positions $-z_{nm}$, as depicted in Fig. 1(b). All those image charges sum up to $-q_n$, as required.

Inside the slab, G_n^- simply corresponds to a series of point charges $(1-\beta)(-\beta)^m q_n, m\geqslant 0$, located at $z_{nm}-2h$ and their mirror images with respect to the back-electrode plane.

B. Electric field profiles

In Fig. 5 we show E_z profiles induced just outside the slab surface and its interface with the back electrode by a point charge. With increasing ϵ, i.e., β, the field above the surface is enhanced, whereas E_z above the back electrode drops because of reduced penetration into the dielectric; concomitantly, the respective half-widths slightly decrease. With increasing h/z_n, $\rho_{1/2}$ increases monotonically at the back-electrode interface

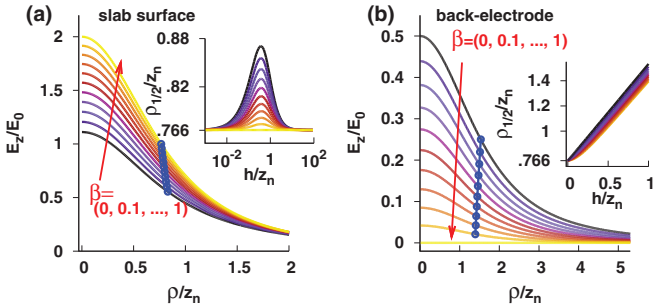

FIG. 5. (Color online) (a) E_z (in units of $E_0=q_n/4\pi\epsilon_0 z_n^2$) vs ρ/z_n just outside the sample for a point charge at z_n above a dielectric slab of thickness $h=z_n$ for several values of β. Blue points indicate the half-width $\rho_{1/2}$ while its variation with h is depicted in the inset; $\rho_{1/2}=0.766z_n$ for $\beta=1$. (b) Same as (a) but just outside the coated back electrode; $\rho_{1/2}=0.766(h+z_n)$ for $\beta=0$.

and stays only slightly below the linear dependence $\rho_{1/2}=\sqrt{2^{2/3}-1}(h+z_n)\simeq 0.766(h+z_n)$ obtained when $\beta=0$. On the sample surface, however, $\rho_{1/2}\simeq 0.766z_n$, apart from a small peak rising to $0.88z_n$ around $h/z_n=0.7$ upon decreasing β. This behavior can be related to the spreading of field lines emanating from q_n at a given angle which end perpendicular to the sample surface if $\beta=1$, but perpendicular to the back electrode otherwise and remain between those for $\beta=1$ and $\beta=0$ (vacuum instead of dielectric layer).

For a biased sphere centered at $z_1=s+R$, Fig. 2(a) shows a more pronounced field enhancement caused by the image charges $q_{n>1}$ closer to the surface, and $\rho_{1/2}$ is somewhat smaller, except when $\beta\to 0$, but this limit corresponds to a missing sample.

IV. SPHERICAL TIP ATOP DIELECTRIC SLAB

In the problem of a biased conducting sphere against a finite dielectric slab, each q_n inside the sphere generates an infinite series of images on the slab side at positions $-z_{nm}$, and each of those induces an image closer to the sphere center to bring it towards an equipotential. The images within the sphere are recursively given by

$$Q(m,q_n,z_n) = \begin{cases} q_n\beta R/(z_1+z_n), & m=-1, \\ q_n(1-\beta^2)(-\beta)^m R/(z_1+z_{nm}), & m\geqslant 0, \end{cases} \tag{23}$$

$$Z(m,z_n) = z_1 - \frac{R^2}{z_1+z_{nm}}. \tag{24}$$

When $h\to\infty$ or $\beta=1$, all images vanish except $Q(-1,q_n,z_n)=q_{n+1}$ and Eqs. (1) and (2) are recovered. Now, to solve the combined sphere-slab problem, one puts the first point charge $q_1=4\pi\epsilon_0 RV$ at the sphere center $z_1=R+s$. An infinite series of images $Q(m,q_1,z_1)$ is then induced inside the sphere, each of which has in turn infinite images $Q[l,Q(m,q_1,z_1),Z(m,z_1)]$ and so on. In a numerical treatment, the infinite series can be truncated as soon as Q becomes small enough. For relevant parameters, Q is at least 10^{-16} times smaller than q_1 when $m>10$; for the same reason only a limited number of nested sums must be considered. In Fig. 6 we illustrate the convergence of our procedure for a

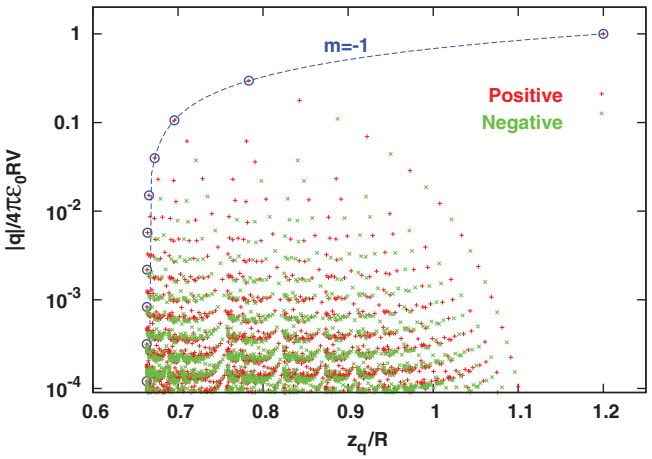

FIG. 6. (Color online) The normalized magnitudes of image charges vs their positions generated within a conducting sphere of radius R at a distance $s = 0.2R$ from an NaCl slab ($\beta = 0.71$) of thickness $0.2R$. The largest point charge of magnitude one is at the sphere center ($z_1 = 1.2R$), while no charges appear below $z_\infty = 0.66R$, z being measured from the slab surface. The first series of image charges given by Eq. (23) with $m = -1$ are shown with circles and define an h-independent upper bound. Further charges with magnitudes larger than 10^{-4} are shown in red (positive) and green (negative).

particular example. The normalized capacitance of the system is $C/\pi\epsilon_0 R = 7.22$ compared to 5.86 and 7.46 in the case of a semi-infinite slab and a perfect conductor, respectively, as given by Eq. (9).

A. Capacitance

The capacitance C is obtained from the total charge on the sphere, namely

$$CV = q_1 + \sum_{m=-1}^{\infty} Q(m,q_1,z_1) + \sum_{l,m=-1}^{\infty} Q[l,Q(m,q_1,z_1),Z(m,z_1)] + \cdots. \quad (25)$$

A systematic summation of the resulting nested series with a prescribed precision is possible as described above. The resulting dependence of the capacitance of the sphere-slab system as a function of s/R and h/R is depicted in Fig. 7. First of all, the dashed lines in Fig. 7(a) show that for $\beta = 1$, Eq. (17) agrees within 2% over the whole examined range of s/R. With increasing s/R, C first becomes almost independent of β at a value which grows with h/R, then approaches the capacitance $C_{\rm sph}$ of the isolated sphere as $2\pi\epsilon_0 R^2/s$. Similarly, at large h/R, C approaches values given by Eq. (9) shown by dashed lines on the right side in Fig. 7(b). The slow approach reflects the influence of the additional image charges. Note that $\beta = 1$ and 0 correspond to a biased sphere at respective separations s and $s + h$ from a perfect conductor.

A smooth interpolation between those two limits is obtained by *replacing* s *with* $s + h/\epsilon_r$, *where* $\epsilon_r = \epsilon/\epsilon_0$, *while keeping* $\beta = 1$ *in Eq.* (9). As shown by dashed lines on the left side in Fig. 7(b), the resulting approximation is within 1% of the exact $C(s/R,h/R)$ for $h \leqslant R/3$ if $s = R/10$. For larger separations $s \sim R$ the deviation remains within 1% as long as $h \leqslant R$, see Fig. 7(c). In view of its remarkable agreement with Eq. (9) for $\beta = 1$, *Eq.* (17) *together with the same substitution provides an almost as good but simple approximation to the exact* C *for small enough* h/R. The same combination $s + h/\epsilon_r$ appears in the denominator of C in the case of a parallel-plate capacitor of thickness $s + h$ partially filled with a dielectric slab of thickness h. However, the proposed approximation remains valid when the field profiles at the top and bottom surfaces of the dielectric slab are far from uniform, e.g., if $s \ll h < R$. This is evidenced by the $E_z(\rho)$ profiles and by their respective half-widths as discussed in the following.

B. Electric field profiles

The electric field profiles for a conducting sphere atop a dielectric slab are shown in Figs. 8 and 9. To compute $E_z(\rho,z) = -\sum q_k \partial_z G_k^{\pm}/4\pi\epsilon_0$, where the GF is given by Eqs. (20) and (21), we used the same point charges q_k which are kept in evaluating Eq. (25) as shown in Fig. 7. With increasing β, the field just outside the surface is enhanced, whereas E_z just above the back electrode drops because of reduced penetration

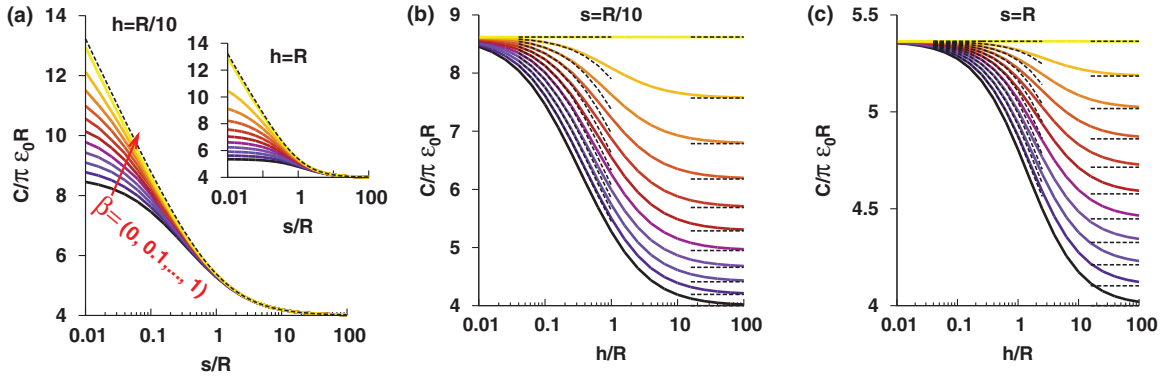

FIG. 7. (Color online) Computed normalized capacitance (a) vs s/R for $h = R/10$ and $h = R$ (inset) and vs h/R for $s = R/10$ (b) and $s = R$ (c) of a conducting sphere of radius R separated by s from a dielectric slab of thickness h. In (a) the dashed lines correspond to Eq. (17). In (b) and (c) the dashed lines on the left correspond to a sphere at an effective separation $s + h/\epsilon_r$ from the back electrode (see text) and those on the right to the sphere at separation s from a semi-infinite dielectric.

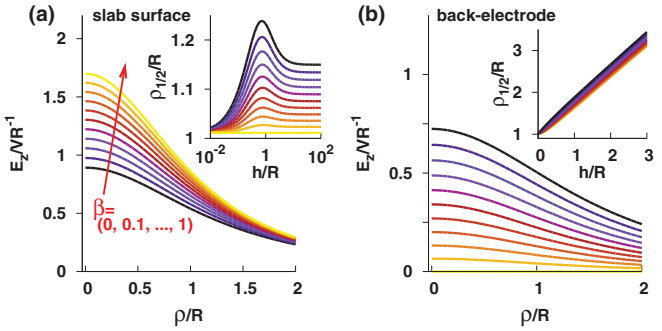

FIG. 8. (Color online) Computed field profiles just outside the sample surface (a) and the back electrode (b) for a conducting sphere of radius R at a separation $s = R/2$ from a dielectric slab of thickness $h = R/2$. The corresponding half-widths $\rho_{1/2}$ as functions of h/R are shown in the insets.

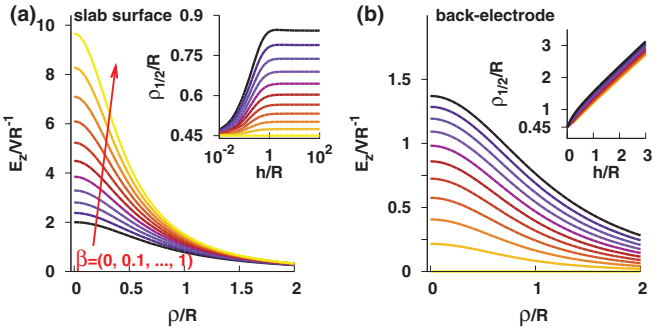

FIG. 9. (Color online) Same as Fig. 8, but for $s = R/10$ [cf. Fig. 2(a)].

into the dielectric. Concomitantly, the respective half-widths slightly decrease.

At the sample surface [insets of Figs. 8(a) and 9(a)], $\rho_{1/2}$ decreases towards values matching those in Fig. 2(b) at the same s if $h \to \infty$, but towards a common value which agrees with that in Fig. 2(b) for $\beta = 1$ if $h \to 0$. A weak maximum consequently appears, around $h \sim R$ which, however, is absent if $s = 0.1R$. If β is close to 1 (undoped or depleted semiconductor capping layer), $\rho_{1/2}$ remains close to the $\beta = 1$ value for all h. Thus, like in Fig. 2(b), the half-widths at the surface are significantly below R, while their spread increases, if s/R is small. At the back-electrode interface [insets of Figs. 8(b) and 9(b)], $\rho_{1/2}$ increases monotonically with increasing h/R and stays below the line $\rho_{1/2} = 0.766(s + R + h)$ obtained when $\beta = 0$ for a lumped charge at the sphere center, as illustrated in the inset of Fig. 5(b), albeit at the separation $s + h$ from the back electrode. Therefore, this line is approached only if $s + h$ becomes comparable to R. In the opposite limit, $\rho_{1/2} \simeq \sqrt{2(s + h)R}$, in accordance with Fig. 2(b). When $h \to 0$ (missing dielectric layer) the half-widths on the back electrode and on the surface coincide with the $\beta = 1$ values in Fig. 2(b), namely $\rho_{1/2}/R = 1.02$ if $s = R/2$ and 0.45 if $s = R/10$. Nevertheless $\rho_{1/2}$ at the back electrode considerably exceeds the half-width at the surface in the common experimental situation when the closest approach distance $s \ll h \leqslant R$.

V. CONCLUSIONS

In summary, using the method of image charges for a biased model spherical tip facing a semi-infinite dielectric, we found a simple generalization of the solution for the sphere-planar conductor problem. Approximate, but accurate compact formulas were obtained for the capacitance and related quantities of current interest in scanning gate or scanning capacitance experiments on doped semiconductors or 2DEGs capped by insulating layers, besides electrostatic force microscopy of insulating thin films on metal substrates. Note that the tip is typically oscillated at or close to a resonance frequency of the force sensor used to control the closest approach distance; probed quantities must therefore be averaged over the tip trajectory.[3,14] Green's functions for field points above and inside a dielectric slab with finite thickness grounded at the bottom were used to setup a systematic numerical solution. For experimentally relevant situations, where the tip apex radius exceeds the tip-sample separation s and the slab thickness h, our numerical results are within 1% of the total capacitance for the sphere-planar conductor problem at an effective separation $s + h/\epsilon_r$. The computed field profile widths at the slab surface and at the back-electrode interface indicate that the common assumption of a tip-surface capacitor in series with a sample capacitor of effective radius comparable to the tip apex radius R is seldom justified. We recommend instead to use the above-mentioned approximation. A worthwhile next step would be to include screening by nonideal conductors, e.g., buried 2DEGs or surface layers, e.g., graphene or metallic surface states.

ACKNOWLEDGMENTS

This work has been supported by the Swiss National Science Foundation (SNF) and the Swiss National Center of Competence in Research (NCCR) on Nanoscale Science. A.B. thanks Andreas Baumgartner for discussions about 2DEG investigations.

*ali.sadeghi@unibas.ch

[1] G. Binnig, H. Rohrer, C. Gerber, and E. Weibel, Appl. Phys. Lett. **40**, 178 (1982).

[2] G. Binnig, C. F. Quate, and C. Gerber, Phys. Rev. Lett. **56**, 930 (1986).

[3] F. J. Giessibl, Rev. Mod. Phys. **75**, 949 (2003).

[4] S. Kalinin and A. Gruverman, *Scanning Probe Microscopy: Electrical and Electromechanical Phenomena at the Nanoscale* (Springer, New York, 2007), Vols. I and II.

[5] J. M. R. Weaver and D. W. Abraham, J. Vac. Sci. Technol. B **9**, 1559 (1991).

[6] M. Nonnenmacher, M. P. O'Boyle, and H. K. Wickramasinghe, Appl. Phys. Lett. **58**, 2921 (1991).

[7] J. Kopanski, J. Marchiando, and J. Lowney, J. Vac. Sci. Technol. B **14**, 242 (1996).

[8]M. Suddards, A. Baumgartner, M. Henini, and C. Mellor, New J. Phys. **14**, 083015 (2012).
[9]M. Topinka, B. LeRoy, S. Shaw, E. Heller, R. Westervelt, K. Maranowski, and A. Gossard, Science **289**, 2323 (2000).
[10]A. Pioda, S. Kičin, T. Ihn, M. Sigrist, A. Fuhrer, K. Ensslin, A. Weichselbaum, S. E. Ulloa, M. Reinwald, and W. Wegscheider, Phys. Rev. Lett. **93**, 216801 (2004).
[11]S. Hudlet, M. Saint Jean, C. Guthmann, and J. Berger, Eur. Phys. J. B **2**, 5 (1998).
[12]C. Barth, T. Hynninen, M. Bieletzki, C. R. Henry, A. S. Foster, F. Esch, and U. Heiz, New J. Phys. **12**, 093024 (2010).
[13]G. M. Sacha, E. Sahagún, and J. J. Sáenz, J. Appl. Phys. **101**, 024310 (2007).
[14]A. Sadeghi, A. Baratoff, S. A. Ghasemi, S. Goedecker, T. Glatzel, S. Kawai, and E. Meyer, Phys. Rev. B **86**, 075407 (2012).
[15]J. D. Jackson, *Classical Electrodynamics* (Wiley, New York, 2001), Chaps. 2 and 4.
[16]F. Bocquet, L. Nony, and C. Loppacher, Phys. Rev. B **83**, 035411 (2011).
[17]L. Nony, A. S. Foster, F. Bocquet, and C. Loppacher, Phys. Rev. Lett. **103**, 036802 (2009).
[18]G. D. Wilk, R. M. Wallace, and J. M. Anthony, J. Appl. Phys. **89**, 5243 (2001).
[19]W. R. Smythe, *Static and Dynamic Electricity*, 2nd ed. (McGraw-Hill, New York, 1950), Chap. 5.
[20]S. Gómez-Moñivas, L. S. Froufe-Pérez, A. J. Caamaño, and J. J. Sáenz, App. Phys. Lett. **79**, 4048 (2001).
[21]L. Kantorovich, A. Foster, A. Shluger, and A. Stoneham, Surf. Sci. **445**, 283 (2000).
[22]S. F. Lyuksyutov, R. A. Sharipov, G. Sigalov, and P. B. Paramonov, arXiv:cond-mat/0408247.
[23]These conditions are not satisfied by the GF proposed for $z > 0$ in Ref. 13.